

Original Article

Open Access



Essential neural anatomy for creating a clinically translatable osseointegrated neural interface for prosthetic control in sheep

Kirsten A. Gunderson¹, Scott K. Odorico¹, Zeeda H. Nkana¹, Lucas Sears¹, Grant Seils¹, Rashea L. Minor², Weifeng Zeng¹ , Samuel O. Poore¹, Aaron M. Dingle¹

¹Division of Plastic Surgery, University of Wisconsin School of Medicine and Public Health, Madison, WI 53792, USA.

²University of Wisconsin-Madison School of Veterinary Medicine, Madison, WI 53706, USA.

Correspondence to: Dr. Aaron. M Dingle, Division of Plastic and Reconstructive Surgery, University of Wisconsin School of Medicine and Public Health, 600 Highland Avenue, CSC G5/347, Madison, WI 53792, USA. E-mail: dingle@surgery.wisc.edu

How to cite this article: Gunderson KA, Odorico SK, Nkana ZH, Sears L, Seils G, Minor RL, Zeng W, Poore SO, Dingle AM. Essential neural anatomy for creating a clinically translatable osseointegrated neural interface for prosthetic control in sheep. *Plast Aesthet Res* 2023;10:50. <https://dx.doi.org/10.20517/2347-9264.2023.42>

Received: 18 May 2022 **First Decision:** 10 Aug 2023 **Revised:** 24 Aug 2023 **Accepted:** 6 Sep 2023 **Published:** 13 Sep 2023

Academic Editors: Joseph M. Rosen, Alison K. Snyder-Warwick **Copy Editor:** Yanbing Bai **Production Editor:** Yanbing Bai

Abstract

Aim: Ovine models for osseointegrated prosthetics research are well established, but do not consider neural control of advanced prostheses. The validity of interfacing technologies, such as the Osseointegrated Neural Interface (ONI), in their ability to provide communication between native nerves and advanced prosthetics is required, necessitating a stable, longitudinal large animal model for testing. The objective of this study is to provide a detailed anatomic description of the major nerves distal to the carpal and tarsal joints, informing the creation of a chronic ONI for prosthetic control in sheep.

Methods: Six pelvic and six thoracic cadaveric limbs from mature female, non-lactating sheep were utilized. Radiographs were obtained to determine average bone length, medullary canal diameter, and cortical bone thickness. Microsurgical dissection was performed to discern topographical neuroanatomy and average circumferences of the major nerves of the pelvic and thoracic limbs. Histologic analysis was performed. A surgical approach for the creation of ONI was designed.

Results: Average metacarpal and metatarsal length was 15.0 cm (\pm 0.0) and 19.7 cm (\pm 1.0), respectively. Average intramedullary canal diameter was 12.91 mm (\pm 3.69) for forelimbs and 12.60 mm (\pm 3.69) for hindlimbs. The thoracic limb nerves consisted of one dorsal and three ventral nerves, with an average circumference of 5.14 mm



© The Author(s) 2023. **Open Access** This article is licensed under a Creative Commons Attribution 4.0 International License (<https://creativecommons.org/licenses/by/4.0/>), which permits unrestricted use, sharing, adaptation, distribution and reproduction in any medium or format, for any purpose, even commercially, as long as you give appropriate credit to the original author(s) and the source, provide a link to the Creative Commons license, and indicate if changes were made.



(± 2.00) and 5.05 mm (± 1.06), respectively. Pelvic limb nerves consisted of two dorsal and one ventral nerve with an average circumference of 6.27 mm (± 1.79) and 5.40 mm (± 0.53), respectively.

Conclusions: These anatomic data inform the surgical approach and manufacture of a sensory ONI for chronic testing in awake, freely ambulating animals for future clinical translation.

Keywords: Amputation, prosthesis, prostheses, neural interface, clinical translation, large animal, osseointegration, neuroprosthesis

INTRODUCTION

The use of large animals as preclinical models is a key step in the translation of biomedical research towards their ultimate application in human patients. Robust, long-term simulation in large animal models is essential to adequately assess the safety and function of any device or intervention prior to human testing. There have been recent technological advances in methods of neural interfacing, such as the Osseointegrated Neural Interface (ONI), which have profound implications for the human amputee population. These interfaces, in combination with advanced prostheses, hold the promise of bi-directional communication in the form of intuitive motor control and sensory feedback between an amputee and their prosthesis; the validity of these new technologies to provide chronic and stable communication between native nerves and advanced prosthetics is required^[1-3]. Dingle *et al.* have demonstrated the durability of ONI in a rabbit model, but furthering this objective requires longitudinal studies in a clinically translatable large animal model^[3-4].

Analysis of currently available animal models in neural prosthetic interfacing was recently performed by Aman *et al.* This article identified that many pilot studies utilize the rat model and rabbit model. Many limitations to these smaller animal models were discussed, including biological differences between rats and humans as well as high infection and self-mutilation rates in rabbit models. Most importantly, though, more comparable anatomy is required to test human-sized devices in a model over time to prove their safety, longevity, and efficacy, which is not possible in small animal models. This article identified a relative dearth of large animal models for the chronic evaluation of peripheral neural interfacing, with no published large animal models for the evaluation of Osseointegrated Neural Interfacing^[5].

One ungulate model has been published. Clites *et al.* demonstrated the utility of a caprine (goat) transtibial and transfemoral hindlimb amputation model for the evaluation of agonist-antagonist myoneural interfacing for prosthetic control. This study demonstrated the chronic stability and safety of an osseointegrated prosthetic device up to day 190 in transfemoral amputation, showing promise for this model in the field of ONI^[6]. Similarly, ovine (sheep) models are well established for osseointegrated prosthetics (OI) research^[7-10]. Adult sheep share a similar size, weight, and bone structure to adult humans, and thus are an accepted large-animal model for bone and implant biomechanics^[11]. The standard ovine model for osseointegration consists of a metacarpal amputation of the thoracic limb as an analogy for transtibial amputation in humans. The ovine model has become the gold standard for long-term large animal OI evaluation, with studies showing stability of at least two years^[7]. It follows, then, that the gold standard for ONI using OI prostheses should be this same clinically robust model: the sheep.

Existing OI ovine models do not consider the implications for neural control of the advanced prosthesis. While there are generalized topographical maps of the nerves of the thoracic and pelvic limbs of sheep, more granular information, particularly distal to the carpal and tarsal joints where the amputation is performed, is lacking. The data are crucial for creating a suitable osseointegrated prosthesis with sensory

feedback based on the relative sheep models of osseointegration.

The purpose of this study is to elucidate the neural topography in the metatarsi and metacarpi of sheep relative to the common amputation sites for osseointegration research in ungulates. The data obtained from this anatomical study will then be utilized to develop a surgical design for creating an osseointegrated neural interface in a clinically translatable sheep model, alongside similar anatomical studies in humans for direct comparison^[12].

METHODS

This work was not conducted with living animals or human subjects. No ethical approval was required.

Animals

Six pelvic and six thoracic cadaveric limbs from mature female, non-lactating sheep (mixed breeds: Polypay, Tarhee, Dorset) were collected for anatomical study. Both forelimbs (thoracic) and hindlimbs (pelvic) were obtained from previous studies, fresh frozen prior to dissection in a standard freezer at -20 °C. No embalming fluid was used for preservation.

Radiological evaluation of the metacarpal and metatarsal bones

Limbs disarticulated at the carpal and tarsal joints were imaged in pairs using a portable digital radiography system (VetRocket, Santa Clara, CA, USA) including an Elkin EDR3 (Sound, Carlsbad, CA), Canon CXDI-31 plate (Canon USA, Inc., Melville, NY, USA) and a min-X HF100/30+ generator (MinXray, Inc, Northbrook, IL, USA). Each limb was radiographed in the medial-lateral transverse plane alongside a 10 cm radiological scale bar. Measurements of metatarsal and metacarpal bones were made using the straightline tool in ImageJ (NIH, Bethesda, MD), with the scale set according to the scale bar present in each image. Horizontal measurements of the dorsal and palmar cortex bone thickness and medullary canal diameter were made at the proximal, midpoint, and distal positions, as demonstrated in [Figure 1](#). All measurements were made in triplicate and averaged to limit human error. Vertical measurements of bone length were made in the medial plane during microsurgical dissection measuring from the proximal point (carpal/tarsal joint) to the distal point (MP joint), as these anatomic landmarks are more easily identifiable intraoperatively relative to exposed nerves.

Microsurgical dissection of the nerves distal to the carpal and tarsal joints

Microsurgical dissection was performed by a single author (K.G.) with the assistance of other authors (W.Z., S.O., Z.N.) to determine the overall topography of the major nerves of the pelvic (superficial fibular, deep fibular, and tibial) and thoracic limbs (superficial radial, dorsal ulnar, deep ulnar, and median) along the metatarsi and metacarpi, respectively. The anatomical locations were selected for their relative positioning to the common amputation site for osseointegration models in sheep, measuring and annotating branch points of each nerve to determine viable interfacing targets for creating an ONI. Limbs were dissected using clean, non-sterile microsurgery equipment (Roboz Surgical Instrument Company, MD, USA; Dumont Switzerland, CH) with a Zeiss West Germany Universal Microscope (S3, 175348; NY, USA). Two researchers were present at every dissection to ensure proper measurement recording and nerve identification. Nerve circumferences were measured at three sites along the metatarsus or metacarpus: the most proximal point (at the carpal/tarsal joint), the midpoint (halfway between the carpal/tarsal and interphalangeal (IP) joints), and the most distal point (IP joint). Measurements were made by wrapping a 7-0 suture circumferentially around each nerve and subsequently measuring the suture. Each measurement was made in triplicate and averaged to ensure accurate measurement and limit human error. Illustrations of the variations in nerve branching patterns were made.



Figure 1. Radiological Evaluation of the Metacarpal and Metatarsal Bones. Example radiograph used to obtain skeletal anatomic measurements. Red dashed lines demonstrate the level at which measurements were made, i.e., proximal, midpoint, and distal metacarpal or metatarsi. Blue line indicates intramedullary diameter. Yellow line indicates cortical thickness.

Morphological examination of the nerves distal to the carpal and tarsal joints

Histological analysis was performed on nerve sections stained with Gomori's trichrome to identify epineurial thickness and number of fascicles for each nerve as previously reported^[3,4,13]. In brief, 1cm samples of each nerve were taken at the proximal, midpoint, and distal positions. Proximal samples were taken 1cm distal to the proximal landmark, the most proximal landmark being the carpal/tarsal joint crease. Distal samples were taken 1cm proximal to the point where the nerve ends or 1cm proximal to the end of the metacarpus or metatarsus. Midpoint samples were taken from the point directly between the most proximal and distal landmarks. All nerve samples were fixed in 10% neutral buffered formalin at 4 °C overnight and processed through graded alcohols in an automated tissue processor (Sakura VIP 5 Tissue Processor, LabX, Ontario, Canada). Processed samples were cut in half transversely, and the proximal and distal transverse surfaces placed face down and paraffin embedded. Transverse serial sections were taken in 5 μM increments, stained with Gomori's trichrome, and scanned at 20x magnification using a PathScan Enabler IV (Meyer Instruments, Huston, TC, USA). Images were viewed and analyzed using Aperio Image Scope software (v12.3.3.5048, Leica Biosystems, Wetzlar, Germany). Using the freehand selection tool, the entirety of the nerve area was outlined to obtain the total section area (TSA). The number of nerve fascicles was manually counted and the area of each nerve fascicle was measured in the same manner as the TSA. The fascicular area for each nerve was then summed to calculate the total fascicular area (TFA). Average values for TSA, TFA, and number of fascicles were calculated as mean ± standard deviation.

Surgical approach for creation of ONI ovine model

A thoracic cadaveric sheep limb was utilized to test and document the feasibility of the surgical design. The anatomic and histologic data gathered above informed nerve selection and electrode design.

RESULTS

Radiological evaluation of the metacarpal and metatarsal bones

The average intramedullary canal diameter was 12.91 (± 3.69) mm for thoracic limbs and 12.60 (± 3.69) mm for pelvic limbs, with the canal being larger in diameter at the proximal and distal locations than at the midpoints. The average cortical bone thickness was 3.23 (± 0.91) mm in the thoracic limbs and 3.30 (± 0.82) mm in the pelvic limbs [Table 1]. Bone measurements demonstrated an average metacarpal length of 15.0 (± 0.0) cm and an average metatarsal length of 19.7 (± 1.0) cm.

Table 1. Radiological evaluation of the metacarpal and metatarsal bones

Limb - location	Intramedullary diameter (mm)	Cortical thickness (mm)
Thoracic - proximal	14.15	4.05
Thoracic - midpoint	8.72	3.73
Thoracic - distal	15.86	2.52
Pelvic - proximal	15.21	2.92
Pelvic - midpoint	10.43	3.71
Pelvic - Distal	12.16	3.28

Microsurgical dissection of the nerves distal to the carpal and tarsal joints

Thoracic limb nerves consisted of one dorsal (superficial radial) and three ventral nerves (dorsal ulnar, deep ulnar, median), with varying branching patterns, with an average circumference of 5.12 (\pm 1.07) mm dorsally and 4.83 (\pm 1.74) mm ventrally at the midpoint. Branching patterns of a representative sample of limbs, the right thoracic limbs ($n = 3$) and right pelvic limbs ($n = 3$) of each animal are demonstrated in [Figure 2](#). The nerve circumference of each branching nerve at three locations along the metacarpus is demonstrated in [Table 2](#).

On the ventral thoracic limb, the median nerve, deep ulnar nerve, and dorsal ulnar nerve are always present at the proximal point, listed from medial to lateral in their positions in the horizontal plane. The median nerve course is quite consistent. It traversed straight down the ventral metacarpus and reliably branched distal to the midpoint but proximal to the distal point into a medial and lateral branch. Additionally, there is a communicating nerve branch that connects from the median nerve to the deep branch of the ulnar nerve just distal to the midpoint in every animal.

The deep branch of the ulnar nerve began superficially and dove deep beneath a fibrinous sheath to course the length of the metacarpus without branching.

The dorsal branch of the ulnar nerve begins its course on the metacarpus on the ventral side and runs along the lateral edge of the bone, sometimes coursing further onto the dorsal aspect of the limb. The nerve branches into a shorter branch named the terminating branch of the dorsal branch of the ulnar nerve, as well as a longer branch, named the long branch of the dorsal branch of the ulnar nerve, in all but one limb. The branching point was sometimes proximal to the midpoint and other times distal to the midpoint.

On the dorsal thoracic limb, half of the limbs began with a single superficial radial nerve that branched just after the proximal point into a lateral and central branch of the dorsal common digital nerve. Subsequently, one of these then branched once more and traversed distally as the central, medial, and lateral branches of the dorsal common digital nerve. On the other half of the limbs, the superficial radial nerve branched just above the proximal point into the superficial radial nerve proper and the medial branch of the superficial radial nerve. While the superficial radial nerve properly branched as it had in the other limbs into the medial, lateral, and central branches of the dorsal common digital nerves, this medial branch of the superficial radial nerve reliably never branched and continued its course down the metacarpus.

Pelvic limb nerves consisted of two dorsal nerves (superficial and deep fibular) and one ventral (tibial) nerve. Nerves had an average circumference of 6.27 (\pm 1.79) mm dorsally and 5.40 (\pm 0.53) mm ventrally at the midpoint. Branching patterns of a representative sample of limbs are demonstrated in [Figure 2](#). The nerve circumference of each branching nerve at three locations along the metatarsus is demonstrated in [Table 2](#).

Table 2. Neural anatomy results

Nerve	Position	Number of limbs with this nerve (of total 6 limbs)	Average circumference (mm)	Std
Thoracic limb - dorsal				
Superficial radial nerve	Proximal	3	6.39	0.95
Medial branch of superficial radial nerve	Proximal	3	5.11	0.19
Lateral branch of dorsal common digital nerve	Proximal	3	6	0.6
Medial branch of dorsal common digital nerve	Midpoint	6	5.42	1.61
Medial branch of dorsal common digital nerve	Distal	6	4.47	0.81
Central branch of dorsal common digital nerve	Midpoint	3	4.61	0.7
Central branch of dorsal common digital nerve	Distal	4	4.59	1.23
Lateral branch of dorsal common digital nerve	Midpoint	6	5.08	0.39
Lateral branch of dorsal common digital nerve	Distal	6	4.28	0.74
Thoracic limb - palmar				
Median nerve	Proximal	6	7.25	0.88
Median nerve	Midpoint	6	7.20	0.92
Medial branch of median nerve	Distal	6	6.25	1.52
Lateral branch of median nerve	Distal	6	5.61	0.74
Communicating branch of median nerve	Distal	6	4.86	0.82
Deep branch of ulnar nerve	Proximal	6	4.56	1.05
Deep branch of ulnar nerve	Midpoint	6	3.33	0.56
Deep branch of ulnar nerve	Distal	6	4.42	1.38
Dorsal branch of ulnar nerve	Proximal	6	6.28	1.56
Dorsal branch of ulnar nerve	Midpoint	2	4.42	0.12
Dorsal branch of ulnar nerve	Distal	1	2.67	N/A
Long branch of dorsal ulnar nerve	Distal	5	4.23	0.81
Long branch of dorsal ulnar nerve	Midpoint	4	3.92	1.04
Terminating branch of dorsal ulnar nerve	Midpoint	4	4.79	1.47
Terminating branch of dorsal ulnar nerve	Distal	4	3.78	0.95
Pelvic limb - dorsal				
Superficial fibular nerve	Proximal	6	8.28	1.76
Superficial fibular nerve	Midpoint	6	7.45	2.1
Central branch of dorsal common digital nerve	Distal	5	6.67	0.75
Central/lateral dorsal common digital nerve	Distal	1	4	N/A
Lateral branch of dorsal common digital nerve	Midpoint	6	5.39	1.7
Lateral branch of dorsal common digital nerve	Distal	5	5.17	1.16
Medial branch of dorsal common digital nerve	Midpoint	1	6.5	N/A
Medial branch of dorsal common digital nerve	Distal	3	6.05	1.07
Deep fibular nerve	Proximal	6	6.83	1.54
Central branch of dorsal metatarsal nerve	Midpoint	6	5.92	1.45
Central branch of dorsal metatarsal nerve	Distal	6	4.92	1.32
Medial branch of dorsal metatarsal nerve	Midpoint	1	6.33	N/A

Medial branch of dorsal metatarsal nerve	Distal	1	4.5	N/A
Pelvic limb - plantar				
Tibial nerve	Proximal	6	8.2	0.88
Lateral plantar nerve	Proximal	6	5.31	0.79
Lateral plantar nerve	Midpoint	6	5.53	0.44
Lateral plantar nerve	Distal	6	5.2	1.18
Medial plantar nerve	Proximal	6	6.42	1.33
Medial plantar nerve	Midpoint	6	5.28	0.62
Medial plantar nerve	Distal	6	6	0.82

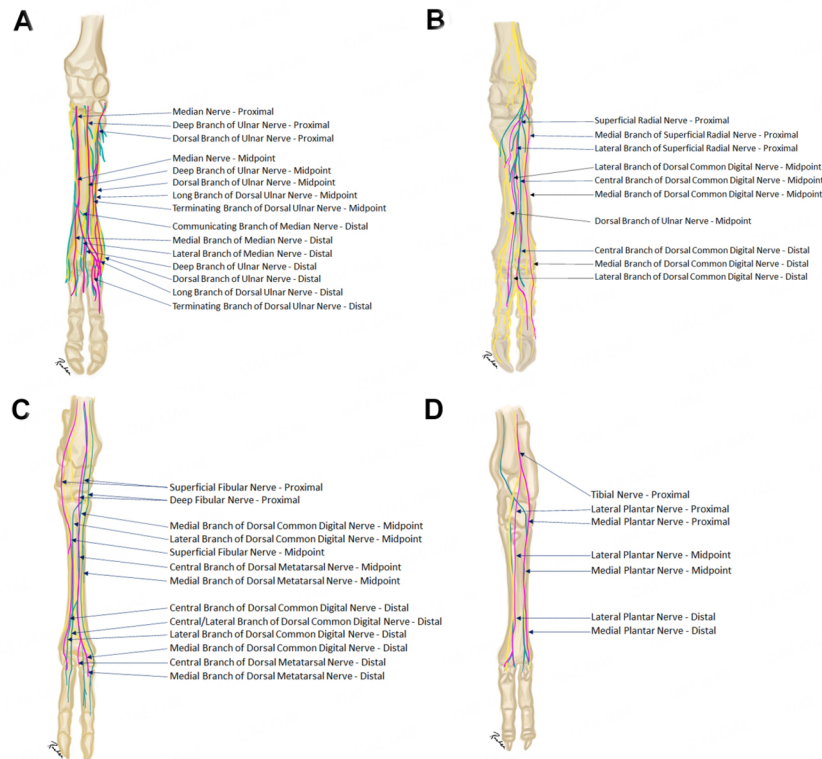


Figure 2. Topographical Neural Anatomy. Representative drawings of topographical neural anatomy of the thoracic (A and B) and pelvic (C and D) sheep limbs in dorsal (A and C) and palmar (B and D) planes. Individual branching patterns of $n = 3$ sheep limbs are demonstrated by different colors.

The ventral pelvic limb had the most consistent neural topography at the level of the metatarsus, with the tibial nerve branching into the lateral plantar and medial plantar nerves. The branching point was always just above the proximal point or within the proximal one-half of the metatarsal.

On the dorsal pelvic limb, the superficial and deep fibular nerves were always present at the proximal point. The superficial fibular nerve branches into the dorsal common digital nerves. Even when it does not branch, by convention, its name is changed to the central branch of the dorsal common digital nerve after the midpoint. The deep fibular nerve branches into the dorsal metatarsal nerves. Even when it does not branch, by convention, its name is changed to the central branch of the dorsal metatarsal nerve at the midpoint. The points of bifurcation of the superficial fibular nerve were widely variable. The deep fibular nerve only bifurcated in one limb. The location of superficial and deep fibular nerves in the horizontal plane at the level

of the tarsal joint varied from animal to animal, as demonstrated in [Figure 2](#).

Morphological examination of the nerves distal to the carpal and tarsal joints

The morphological analysis revealed that the average cross-sectional sample contained a rounded average of 10 fascicles within the extracellular matrix. The median number of fascicles was found to be 8 across all samples. The average fascicular area across all samples was $283,108.35 \mu\text{M}^2$. At $846,645.3 \mu\text{M}^2$, samples of the lateral plantar nerve taken 1cm proximal of the crease of the ankle had the largest average fascicular area. The proximal and distal samples of this nerve had 16 and 13 fascicles, respectively. On average, the fascicular area constituted 15.23% of the total nerve area. The nerve with the greatest fascicular area was the proximal bifurcation of the lateral plantar nerve, constituting 39.43% of the total nerve area. Detailed results of morphological neural analysis can be found in [Table 3](#). Histological cross-sections of a sample of nerves are demonstrated in [Figure 3](#).

Surgical approach for creation of ONI ovine model

A cadaveric sheep forelimb was utilized for demonstration. A nine-centimeter lazy-S incision was created over the proximal dorsal metacarpal. Dissection of loose areolar tissue revealed the primary interdigital sensory nerves in this area, representing the branches of the Superficial Radial Nerve. As demonstrated in our anatomic data, there is more variation in branching patterns of some nerves rather than others, as well as more variation in nerve circumference of some nerves over others. It was found that the Central Branch is often the thickest with the least variation; thus, the Central Branch was chosen as our target nerve for creating a reproducible sensory neural interface in sheep. Target nerve was transected distally, three centimeters from the carpal joint. Soft tissue overlying the bone was cleared using a hemostat and elevator. A primary corticotomy was made 20 mm distal to the carpal joint on the medial side of the bone with a handheld electric drill, using a 3/16th inch (4.76 mm) drill bit. A secondary, smaller corticotomy was made with a 5/32nd inch (3.97 mm) drill bit 1cm lateral to the primary corticotomy. Nerve circumference data were used to inform the correct choice of size for the cuff electrodes, as well as drill size for the corticotomy.

A neural interface consisting of three spiral silicone cuffs [[Figure 4A-Figure C](#)], two of which contain active electrodes [[Figure 4A](#) and [Figure 4B](#)] for stimulation and recording, and a third with no electrodes that serve to stabilize the interface [[Figure 4C](#)], was created as previously described^[14]. Spiral nerve cuff electrodes were used based on availability and applicability, but a range of interfaces are applicable.

Electrode A was attached to the distal end of the transected target nerve. Electrode B was then connected more proximally to the nerve, at a point of minimal tension. The target nerve, concurrently with Electrode A, was then transposed into the medullary canal through the primary corticotomy by threading an epineurial propene suture into the primary corticotomy and out the secondary corticotomy and secured to the periosteum. Electrode B remained outside the medullary canal, maintaining the separation of 10cm necessary for stimulation and recording of compound nerve action potentials between electrodes. The distal electrode (A) can then deliver sensory stimulation to be detected by the proximal electrode (B) in situ. The electrode cables then exit transcutaneously and are anchored with suture.

DISCUSSION

The Osseointegrated Neural Interface is a developing technology with an overarching goal of creating a bidirectional prosthesis capable of both motor control and sensory realization^[12]. This technology has demonstrated success in a small animal model involving rabbits, but longitudinal studies in a large animal model are necessary before translation to human use can be pursued^[3,4]. Building on current clinically translatable ovine models for osseointegration, we studied the topography of ovine nerves distal to the

Table 3. Results of morphological neural analysis

Nerve name	Position	Average nerve area (uM ²)	Standard deviation of nerve area (uM ²)	Average total fascicular area (uM ²)	Standard deviation of total fascicular area (uM ²)	Total fascicular area (%)	Total extracellular matrix (%)
Medial branch radial N.	Proximal	1,313,621.363	412,180.6304	116,159.12	18,430.87697	8.842663742	91.15733626
Central / lateral branch radial N.	Proximal	1,892,015.565	168,331.4299	237,425.4867	82,985.04038	12.54881255	87.45118745
Medial branch radial N.	Midpoint	1,528,413.842	287,019.6112	80,721.845	30,706.83365	5.281412847	94.71858715
Central branch of radial N.	Midpoint	1,550,498.694	951,764.8618	431,248.65	158,927.0151	27.81354488	72.18645512
Lateral branch of radial N.	Midpoint	1,533,614.68	807,205.5485	108,289.55	61,751.90331	7.061066343	92.93893366
Medial branch radial N.	Distal	1,735,489.264	447,020.0519	79,376.4175	47,947.76387	4.573719882	95.42628012
Central branch of radial N.	Distal (3.5 cm distal to midpoint)	1,072,624.97	509,263.4167	82,661.6675	27,200.23345	7.706483609	92.29351639
Lateral branch of radial N.	Distal	1,537,271.872	436,733.9587	79,250.721	15,100.21843	5.155283359	94.84471664
Superficial radial N.	Proximal	2,347,674.918	1,193,555.59	128,505.46	15,423.95929	5.473733139	94.52626686
Branch of terminating branch of dorsal ulnar N.	Midpoint	839,925.775	N/A*	44,004.65	N/A*	5.239111754	94.76088825
Branch of terminating branch of dorsal ulnar N.	Distal	962,672.64	N/A*	64,457.65	N/A*	6.695697719	93.30430228
Central / medial branch of radial N.	Midpoint	2,066,971.175	N/A*	228,208.705	N/A*	11.04072992	88.95927008
Central / lateral branch radial N.	Midpoint	1,596,757.93	N/A*	45,194.945	N/A*	2.830419323	97.16958068
Central / lateral branch radial N.	Distal	1,303,129.315	N/A*	78,874.895	N/A*	6.052729694	93.94727031
Median N.	Proximal	2,406,305.358	1,125,733.976	574,786.6892	237,869.2077	23.8866895	76.1133105
Median N.	Midpoint	2,920,078.987	1,489,425.397	822,654.8525	185,020.2374	28.17234932	71.82765068
Median branch median N.	Distal	1,997,311.363	425,958.1426	766,990.1033	223,089.9885	38.40112852	61.59887148
Lateral branch median N.	Distal	1,483,023.419	746,634.8083	183,019.0279	98,074.25392	12.34093984	87.65906016
Communicating branch of median N.	Distal	1,434,057.461	128,450.834	162,295.6858	65,875.57429	11.3172373	88.6827627
Dorsal branch ulnar N.	Proximal	2,222,570.797	785,671.6911	190,916.405	113,231.3332	8.589890828	91.41010917
Dorsal Branch Ulnar N.	Midpoint	876,619.125	354,876.52	242,544.5325	183,989.7225	27.66817716	72.33182284
Dorsal branch ulnar N.	Distal	540,561.21	N/A*	35,379.02	N/A*	6.544868434	93.45513157
Terminating branch of dorsal ulnar N.	Midpoint	1,060,977.388	181,045.7686	54,620.88625	35,579.1525	5.148166859	94.85183314
Terminating branch of dorsal ulnar N.	Distal	1,560,086.195	896,131.7873	56,645.945	45,989.14068	3.630949699	96.3690503
Long branch of dorsal ulnar N.	Midpoint	1,377,394.735	220,426.1151	125,758.3388	26,724.30042	9.130159681	90.86984032

Long branch of dorsal ulnar N.	Distal	1,438,430.212	282,639.8785	143,960.12	123,698.8446	10.00814074	89.99185926
Deep branch ulnar N.	Proximal	1,141,498.47	784,187.291	117,954.0983	85,557.96491	10.33326819	89.66673181
Deep branch ulnar N.	Midpoint	1,272,470.884	1,024,607.919	212,518.6942	106,468.3658	16.70126184	83.29873816
Deep branch ulnar N.	Distal	1,562,244.878	803,220.2557	278,520.6333	89,729.98326	17.82823149	82.17176851
Tibial N.	1 cm Prox. Of bifurcation of M/L plantar	2,032,110.05	989,502.4044	457,189.5675	157,432.8918	22.49826812	77.50173188
Medial plantar N.	1 cm distal. To ankle crease	2,444,967.505	244,404.68	474,353.615	68,091.135	19.4012237	80.5987763
Lateral plantar N.	1 cm distal to ankle crease	3,001,371.913	1,675,028.723	609,126.86	228,210.965	20.2949477	79.7050523
Medial plantar N.	1 cm Prox. To ankle crease	1,703,571.425	2,257.495	464,374.9125	22,725.9825	27.25890477	72.74109523
Lateral plantar N.	1 cm Prox. To ankle crease	2,884,707.655	525,624.94	846,645.2875	42,027.9875	29.34943116	70.65056884
Medial plantar N.	Distal (at Distal point)	1,573,032.03	86,276.895	313,865.8525	132,873.8875	19.95292191	80.04707809
Lateral plantar N.	Distal (at Distal point)	1,757,430.045	705,338.245	298,924.1175	148,620.4825	17.00916166	82.99083834
Lateral plantar N.	Distal (1 cm Prox. To bifurcation of Lat. Plantar)	1,143,518.22	N/A*	450,854.055	N/A*	39.4269236	60.5730764
Medial plantar N.	Distal (1 cm Prox. To bifurcation of Med. Plantar)	1,150,726.805	N/A*	363,439.995	N/A*	31.58351691	68.41648309
Medial plantar N.	Distal (1 cm Prox. To bifurcation of Lat. Plantar)	1,018,252.33	N/A*	357,795.265	N/A*	35.13817297	64.86182703
Lateral plantar N.	Distal (1 cm Prox. To bifurcation of Med. Plantar)	1,429,746.225	N/A*	232,745.025	N/A*	16.27876479	83.72123521
Tibial N.	Proximal	924,379.7175	34,752.3275	291,907.675	9,556.83	31.57876244	68.42123756
Medial plantar N.	Proximal	2,282,602	591,380.565	397,653.075	6,225.9	17.42104296	82.57895704
Lateral plantar N.	Proximal	3,651,584.443	296,939.8925	597,143.0025	145,304.6625	16.35298353	83.64701647
Medial plantar N.	Mid-point	1,850,289.553	359,026.7493	187,006.1675	47,972.77513	10.10685961	89.89314039
Lateral plantar N.	Mid-point	1,536,098.163	446,599.2818	240,943.665	117,019.211	15.68543409	84.31456591
Medial plantar N.	Distal	1,575,482.758	162,858.6725	324,655.6	27,510.885	20.60673774	79.39326226
Lateral plantar N.	Distal	2,804,900.3	573,914.25	180,291.08	29,036.97	6.427717948	93.57228205
Superficial fibular N.	Proximal	3,576,311.589	1,668,744.949	464,885.5117	234,806.0552	12.99902148	87.00097852
Superficial fibular N.	Midpoint	4,077,167.3	N/A*	629,677.65	N/A*	15.44399834	84.55600166
Superficial fibular N. – lateral branch	Midpoint	2,416,342.753	1,203,104.367	333,369.7033	184,930.617	13.7964576	86.2035424
Superficial fibular N. - lateral branch	Distal	2,085,843.065	470,742.1874	352,372.4317	467,105.6561	16.89352558	83.10647442
Superficial fibular N. - lateral branch	Midpoint	1,813,696.798	202,650.9275	262,851.49	227,605.52	14.49258169	85.50741831
Superficial fibular N. – lateral branch	Distal	2,725,055.395	820,673.1382	332,943.6113	96,991.87522	12.2178658	87.7821342
Deep fibular N.	Proximal	2,252,952.532	964,165.2333	146,231.585	108,294.8549	6.49066427	93.50933573
Deep fibular N.	Midpoint	622,198.445	473,211.6494	170,060.975	117,375.0952	27.33227258	72.66772742
Deep fibular N.	Distal	1,883,652.097	479,382.9502	139,601.88	20,926,102.57	7.411234815	92.58876519

Deep fibular N. – lateral branch	Midpoint	1,224,080.495	N/A*	181,893.49	N/A*	14.85960202	85.14039798
Deep fibular N. – lateral branch	Distal	788,843.18	N/A*	159,294.335	N/A*	20.19340967	79.80659033
Dorsal common digital N. – lateral branch	Midpoint	920,457.27	44741.7	59,917.8625	41,165.3425	6.50957567	93.49042433
Dorsal common digital N. – lateral branch	Distal	2,933,135.915	N/A*	838,514.52	N/A*	28.58764627	71.41235373
Dorsal common digital N.	Midpoint	4,047,344.705	N/A*	0	N/A*	0	100
Dorsal common digital N.	Distal	1,898,824.595	N/A*	256,762.675	N/A*	13.52219029	86.47780971
Superficial fibular N. – central/medial branch	Midpoint	3,944,359.935	N/A*	574,950.025	N/A*	14.57651012	85.42348988
Superficial fibular N. - medial branch	Midpoint	3,625,162.95	N/A*	275,322.86	N/A*	7.594771981	92.40522802
Superficial fibular N. - medial branch	Distal	2,046,172.032	691,991.2229	224,397.5167	250,036.6623	10.96669846	89.03330154
Deep fibular N. – medial branch	Midpoint	1,181,432.77	N/A*	342,545.06	N/A*	28.99403747	71.00596253
Deep fibular N. – medial branch	Distal	1,418,896.3	N/A*	0	N/A*	0	100
Dorsal common digital N. – medial branch	Midpoint	3,508,577.213	283,054.4475	0	N/A*	0	100
Dorsal common digital N. – medial branch	Distal	2,168,133.66	N/A*	234,580.705	N/A*	10.81947618	89.18052382

*These nerves were present in < 3 limbs, negating averages.

carpal and tarsal joints in order to design and create an ONI suitable for chronic testing in sheep. The data herein were consistent with models of ovine OI^[7,8,15].

Bone measurements demonstrate an average metacarpal length of 15.0 (\pm 0.0) cm and an average metatarsal length of 19.7 (\pm 1.0) cm. The average cortical bone thickness was 3.23 (\pm 0.91) mm in the thoracic limbs and 3.30 (\pm 0.82) mm in the pelvic limbs. The average intramedullary canal diameter was 12.91 (\pm 3.69) mm for thoracic limbs and 12.60 (\pm 3.69) mm for pelvic limbs. The thoracic limbs consisted of one dorsal (superficial radial) and three ventral (median, dorsal ulnar, and deep ulnar) nerves, with an average circumference of 5.12 (\pm 1.07) mm and 4.83 (\pm 1.74) mm at the midpoint, respectively. Pelvic limb nerves consisted of two dorsal (superficial fibular and deep fibular) and one ventral (tibial) nerve with an average circumference of 6.27 (\pm 1.79) mm and 5.40 (\pm 0.53) mm at the midpoint, respectively.

At the level of amputation in the classic ovine OI, the distal metacarpus, all nerves provide cutaneous sensory innervation, with no identifiable motor targets, and thus are the ideal target nerves for the creation of osseointegrated prosthesis with sensory feedback. Nerves were adequate in both length and circumference to support the creation of a neural interface with subsequent transposition into the medullary canal.

Sheep transmetatarsal amputation is the gold standard in OI research, representative of human transtibial amputation. The forelimb anatomy and joint loading are more similar to the human knee joint than that of

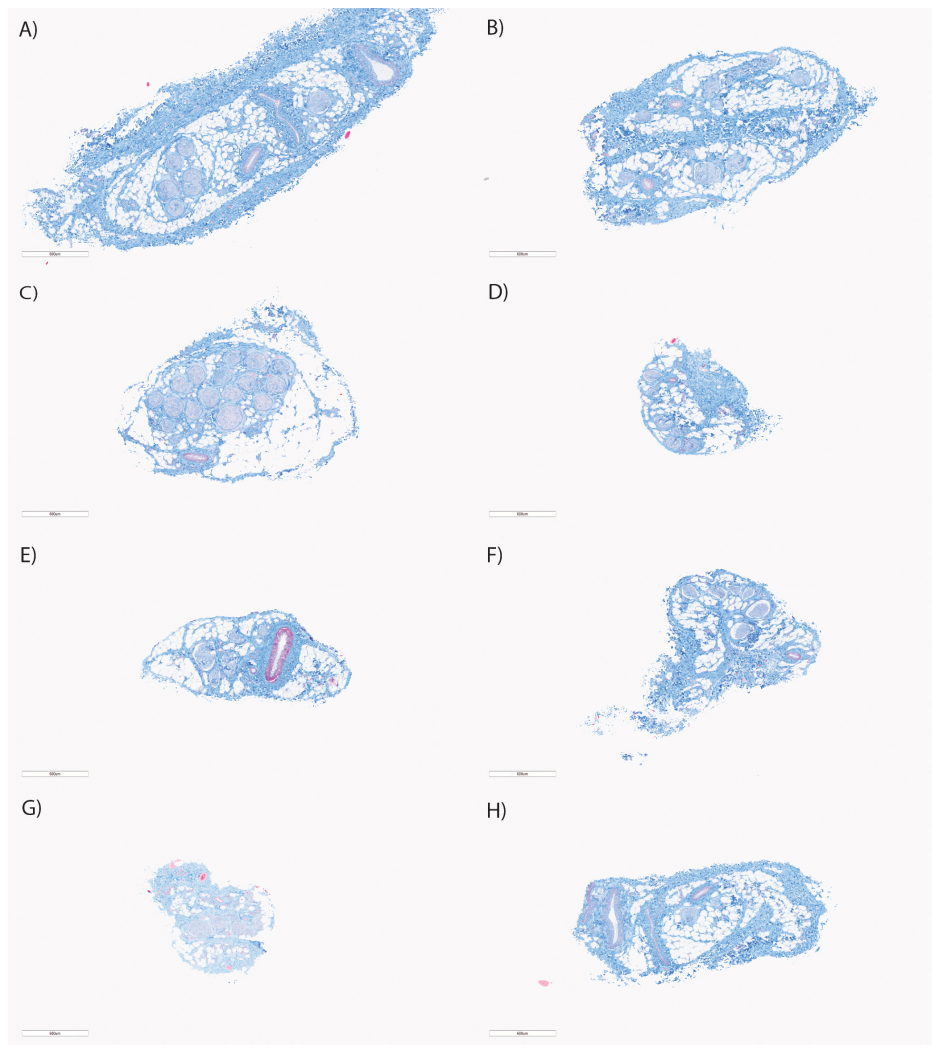


Figure 3. Histological Cross-Sections. Representative micrographs of the nerves of the dorsal aspect of the ovine thoracic limb from a single animal (Proximal to distal). (A) Superficial radial nerve; (B) Lateral branch of the radial nerve; (C) Central branch of the radial nerve; (D and E) Branches of the terminating branch of the dorsal ulnar nerve; (F) Lateral branch of the dorsal common digital nerve; (G) Central branch of the dorsal common digital nerve; (H) Medial branch of the dorsal common digital nerve. Stain: Gomori's trichrome. Magnification x4, scale bar = 600 μ M.

the hindlimb, which is remarkably complex. The standing orientation of the forelimb is more vertical than that of the hindlimb and provides more even loading of the OI implant^[16,8,10,17]. Further, equines and ovines have a unique stay apparatus in their hindlimbs, which negates the use of the hindlimb as a load-bearing model for prostheses. This apparatus is a delicate balance of tendons, ligaments, and muscles that both passively and actively allow them to remain upright with minimal energy consumption^[18,19]. If these are transected in the hindlimb, as is the case during amputation, the animal will refuse to bear weight on the limb entirely.

Caprines (goats) do not have such a stay mechanism, which makes a hindlimb model possible, as Clites *et al.* have demonstrated^[6]. However, the caprine model has not been proven in longevity and consistency as has the sheep model, particularly in the realm of OI. Additionally, sheep weight, size, and bony remodeling have been demonstrated to be acceptably similar to that of humans, with specific data



Figure 4. Surgical Approach. Left: Neural interface. Electrode A is an active electrode capable of delivering sensory stimulation signals. Electrode B is an active electrode, which detects sensory stimulation delivered by Electrode A. Electrode C is a stabilizing electrode. Ruler in image 1 measures millimeters. Right: Image of surgical dissection, as described in text. Electrode A is intramedullary in this photo. Electrode C is not included in this surgical demonstration. Ruler in image 2 measures centimeters.

surrounding OI prosthetics. These data are lacking for the caprine model. Thus, sheep provide a more accurate and reliable translational model, specifically for OI research. It stands that this would be the appropriate model for ONI research, as well.

There are several different types of OI prostheses – Osseointegrated Prosthesis for the Rehabilitation of Amputees (OPRA), a screw-type prosthesis, Osseointegrated Prosthetic Limb (OPL), and the Integral Leg Prosthesis (ILP), both of which are press-fit prostheses. The proposed model for ONI testing in sheep would be compatible with all of these devices. Importantly, in the surgical approach delineated in this article, it is noted that wires are passed subcutaneously and out of the skin to connect with a recording and stimulating device. In the final design of the osseointegrated neural interface, the communicating wires travel through the osseointegrated implant and communicate with the prosthesis through the osseointegrated abutment^[12]. The e-OPRA implant is a modification of the OPRA implant designed specifically to allow bi-directional interfacing via the medullary canal. Given that the sheep model for OI is well established, the focus of this article was the relevant neural anatomy and surgical approach required to construct the neural interfacing componentry of an ONI.

There are limitations to this study. This study was performed on cadaveric sheep limbs and thus anatomy, specifically nerve circumference, may not be fully representative of the awake and ambulating sheep. Importantly, sheep were fresh frozen and not preserved in formalin or other alcohol in order to preserve anatomy to the highest possible degree. Additionally, the low number of specimens is a limitation. There may be anatomical variations that were not picked up, given the low number of sheep limbs dissected. The study herein provides valuable granular information in two dimensions in space, the proximal/distal and the medial/lateral dimension. However, this study is limited in its ability to provide further data in the anterior to posterior dimension to the audience. Importantly, this dimension was considered during dissection when determining easy and appropriate target nerves for our surgical approach, but granular data

were not collected to provide in text.

CONCLUSIONS

The present study provides essential anatomic data for creating an ovine osseointegrated prosthesis with sensory feedback, based on the accepted gold standard sheep model of osseointegration. These data inform the manufacture of a sensory ONI for chronic testing in awake, freely ambulating large animals for future clinical translation.

DECLARATIONS

Acknowledgments

We would like to acknowledge the University of Wisconsin Surgery Histology Core and the University of Wisconsin Translational Research Initiatives in Pathology group for their assistance with histology slide creation and image analysis.

Authors' contributions

Concept, design, data collection/analysis, manuscript drafting: Gunderson KA, Dingle AM

Concept, design, data collection/analysis, manuscript revision: Odorico SK, Nkana ZH, Zeng W

Data collection/analysis, manuscript revision: Sears L, Seils G

Concept, design, figure creation, manuscript revision: Minor RL

Concept, design, data analysis, manuscript revision: Poore SO

Availability of data and materials

Data and materials from this study will be provided upon request.

Financial support and sponsorship

None.

Conflicts of interest

All authors declared that there are no conflicts of interest.

Ethical approval and consent to participate

In accordance with the University of Wisconsin-Madison Institutional Animal Care and Use Committee's ethics policies, the ethical review was not required to undertake this research.

Consent for publication

Not applicable.

Copyright

© The Author(s) 2023.

REFERENCES

1. Millevolte AXT, Dingle AM, Ness JP, et al. Improving the selectivity of an osseointegrated neural interface: proof of concept for housing sieve electrode arrays in the medullary canal of long bones. *Front Neurosci* 2021;15:613844. DOI PubMed PMC
2. Karczewski AM, Dingle AM, Poore SO. The need to work arm in arm: calling for collaboration in delivering neuroprosthetic limb replacements. *Front Neurobot* 2021;15:711028. DOI PubMed PMC
3. Dingle AM, Ness JP, Novello J, et al. Methodology for creating a chronic osseointegrated neural interface for prosthetic control in rabbits. *J Neurosci Methods* 2020;331:108504. DOI
4. Dingle AM, Ness JP, Novello J, et al. Experimental basis for creating an osseointegrated neural interface for prosthetic control: a pilot study in rabbits. *Mil Med* 2020;185:462-9. DOI

5. Aman M, Bergmeister KD, Festin C, et al. Experimental testing of bionic peripheral nerve and muscle interfaces: animal model considerations. *Front Neurosci* 2020;13:1422. [DOI](#) [PubMed](#) [PMC](#)
6. Clites TR, Carty MJ, Srinivasan SS, Talbot SG, Brånemark R, Herr HM. Caprine models of the agonist-antagonist myoneural interface implemented at the above- and below-knee amputation levels. *Plast Reconstr Surg* 2019;144:p 218e-229e. [DOI](#) [PubMed](#)
7. Jeyapalina S, Beck JP, Agarwal J, Bachus KN. A 24-month evaluation of a percutaneous osseointegrated limb-skin interface in an ovine amputation model. *J Mater Sci Mater Med* 2017;28:179. [DOI](#)
8. Jeyapalina S, Beck JP, Drew A, Bloebaum RD, Bachus KN. Variation in bone response to the placement of percutaneous osseointegrated endoprostheses: a 24-month follow-up in sheep. *PLoS One* 2019;14:e0221850. [DOI](#) [PubMed](#) [PMC](#)
9. Hoellwarth JS, Tetsworth K, Rozbruch SR, Handal MB, Coughlan A, Al Muderis M. Osseointegration for amputees: current implants, techniques, and future directions. *JBJS Rev* 2020;8:e0043. [DOI](#) [PubMed](#) [PMC](#)
10. Shelton TJ, Beck JP, Bloebaum RD, Bachus KN. Percutaneous osseointegrated prostheses for amputees: limb compensation in a 12-month ovine model. *J Biomech* 2011;44:2601-6. [DOI](#) [PubMed](#) [PMC](#)
11. Sartoretto SC, Uzeda MJ, Miguel FB, Nascimento JR, Ascoli F, Calasans-Maia MD. Sheep as an experimental model for biomaterial implant evaluation. *Acta Ortop Bras* 2016;24:262-6. [DOI](#) [PubMed](#) [PMC](#)
12. Karczewski AM, Zeng W, Stratchko LM, Bachus KN, Poore SO, Dingle AM. Clinical basis for creating an osseointegrated neural interface. *Front Neurosci* 2022;16:828593. [DOI](#) [PubMed](#) [PMC](#)
13. Settell ML, Pelot NA, Knudsen BE, et al. Functional vagotomy in the cervical vagus nerve of the domestic pig: implications for the study of vagus nerve stimulation. *J Neural Eng* 2020;17:026022. [DOI](#) [PubMed](#) [PMC](#)
14. Blanz SL, Musselman ED, Settell ML, et al. Spatially selective stimulation of the pig vagus nerve to modulate target effect versus side effect. *J Neural Eng* 2023;20:016051. [DOI](#) [PubMed](#) [PMC](#)
15. Jeyapalina S, Beck JP, Bachus KN, Chalayon O, Bloebaum RD. Radiographic evaluation of bone adaptation adjacent to percutaneous osseointegrated prostheses in a sheep model. *Clin Orthop Relat Res* 2014;472:2966-77. [DOI](#) [PubMed](#) [PMC](#)
16. Duda GN, Eckert-Hübner K, Sokiranski R, Kreutner A, Miller R, Claes L. Analysis of inter-fragmentary movement as a function of musculoskeletal loading conditions in sheep. *J Biomech* 1998;31:201-10. [DOI](#) [PubMed](#)
17. Grisez BT, Hanselman AE, Boukhemis KW, Lalli TAJ, Lindsey BA. Osseointegrated transcutaneous device for amputees: a pilot large animal model. *Adv Orthop* 2018;2018:4625967. [DOI](#) [PubMed](#) [PMC](#)
18. Schuurman SO, Kersten W, Weijs WA. The equine hind limb is actively stabilized during standing. *J Anat* 2003;202:355-62. [DOI](#) [PubMed](#) [PMC](#)
19. Welsh PJ, Collier CG, Clement HM, Vakula MN, Mason JB. Cranial Cruciate ligament desmotomies in sheep resulting in peroneus tertius injury. *Case Rep Vet Med* 2021;2021:2628791. [DOI](#) [PubMed](#) [PMC](#)